PLASMA PHYSICS GROUP
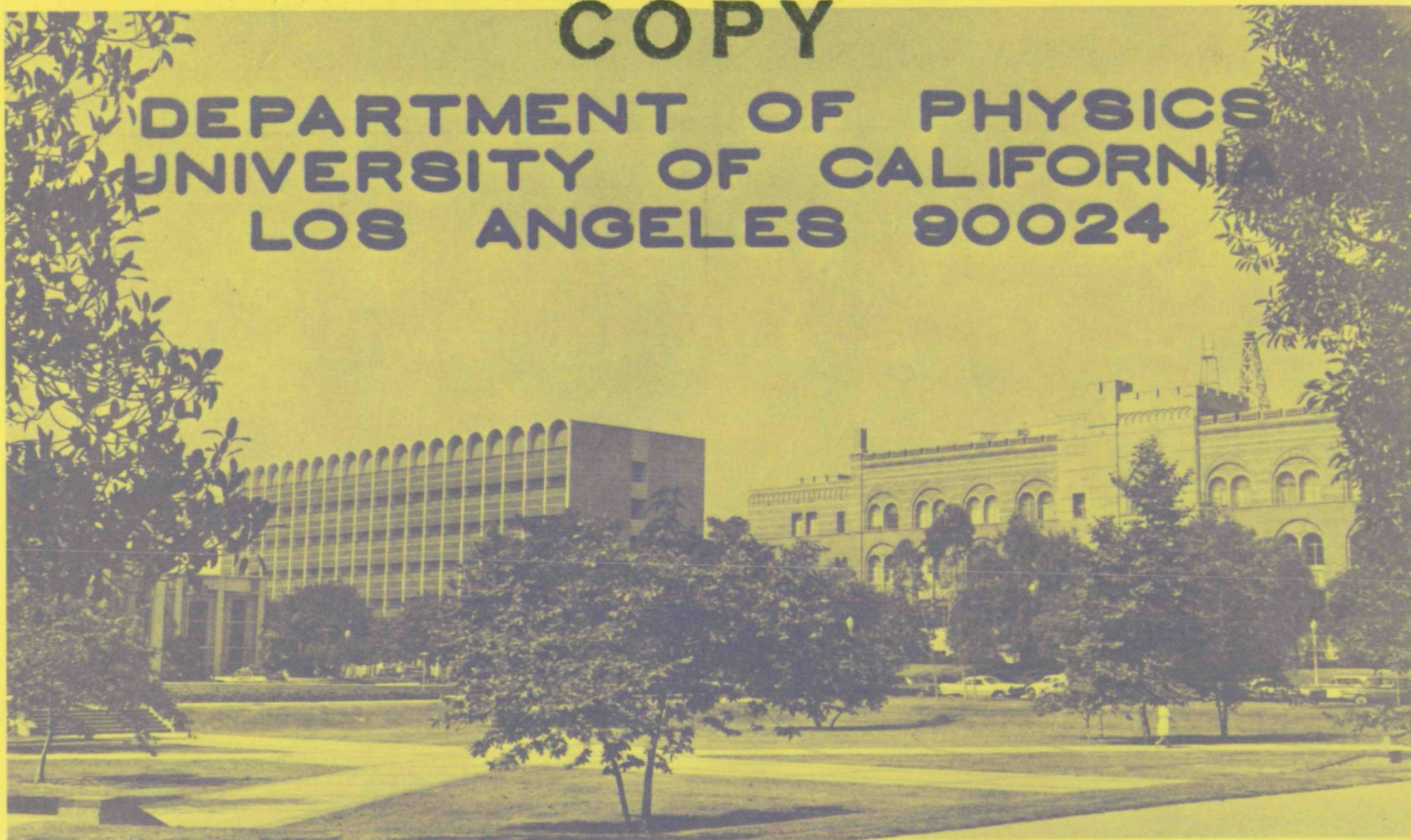
DEPARTMENT OF PHYSICS
UNIVERSITY OF CALIFORNIA
LOS ANGELES 90024

High Frequency Hall Current Instability

K. Lee, C. F. Kennel, J. M. Kindel[*]

N73-10378

Plasma Physics Group
Department of Physics
University of California
Los Angeles, California

[*]Present Address: Plasma Physics Laboratory, Princeton, New Jersey 08540

High Frequency Hall Current Instability

K. Lee, C. F. Kennel, J. M. Kindel

In the auroral zone, VLF hiss observation is a common feature of magnetic substorms. Quite a few years ago Buneman (1963) and Farley (1963) had found that long wavelength electrostatic waves are unstable in the E region of the ionosphere when the relative drift between the ions and electrons exceeds the ion thermal speed. To explore whether or not this Hall current electrojet instability might also generate hiss at VLF frequencies, we have extended their work to shorter wavelengths and higher frequencies. For shorter wavelength modes, electron Debye length corrections can no longer be neglected and the dispersion relation therefore becomes density dependent.

We have assumed the following parameters:

$$B = .5 \, Gauss \; ; \qquad \Omega_E = 8.8 \times 10^{6} \, SEC^{-1} \; ; \qquad \Omega_I = 1.6 \times 10^{2} \, SEC^{-1} \; FOR \; NO^{+}$$

$$T = 230°K \; ; \qquad \nu_{IN} = 1.5 \times 10^{3} \, SEC^{-1} \; ; \qquad \nu_{EN} = 2.6 \times 10^{4} \, SEC^{-1}$$

We have chosen the magnetic field to be .5 gauss so that our calculation will be applicable to the auroral region. Ω_E and Ω_I are the electron and ion cyclotron frequencies respectively. NO^{+} has been assumed to be the only ion species. We have used Farley's temperature and collision frequencies to facilitate comparison with his calculation. We realize this temperature is low for the auroral zone. We have made some calculations with T=460°K and have found no significant changes in the results.

- 1 -

The basic equations are the kinetic equations with particle
conserving Krook collision operator for electrons and ions

$$\frac{\partial f^{+}}{\partial t} + \underline{v} \cdot \nabla f^{+} + \frac{e}{m_{+}} \left(\underline{E} + \frac{\underline{v} \times \underline{B}}{C} \right) \cdot \nabla_{v} f^{+} = - \gamma_{IN} \left[f^{+} - \frac{N_{i}^{+}(\underline{r}, t)}{N_{0}} f_{0}^{+} \right]$$

$$\frac{\partial f^{-}}{\partial t} + \underline{v} \cdot \nabla f^{-} - \frac{e}{m_{-}} \left(\underline{E} + \frac{\underline{v} \times \underline{B}}{C} \right) \cdot \nabla_{v} f^{-} = - \gamma_{EN} \left[f^{-} - \frac{N_{i}^{-}(\underline{r}, t)}{N_{0}} f_{0}^{-} \right]$$

and Poisson's equation

$$\nabla \cdot \underline{E} = 4 \pi e \int (f^{+} - f^{-}) \, d^{3}\underline{v} \; ; \qquad f^{\pm} = f_{1}^{\pm} + f_{0}^{\pm}$$

$$f_{0}^{+} = \frac{N_{0}}{\pi^{3/2} a_{I}^{3}} e^{-\frac{v^{2}}{a_{I}^{2}}} \; ; \qquad f_{0}^{-} = \frac{N_{0}}{\pi^{3/2} a_{E}^{3}} e^{-\frac{(v_{x} - v_{d})^{2} + v_{y}^{2} + v_{z}^{2})}{a_{E}^{2}}}$$

$$V_{d} = \frac{C E}{B} \; ; \quad N_{i}^{\pm} = \int f_{1}^{\pm} \, d^{3}\underline{v}$$

The linearized kinetic equation can be fourier transformed and the
perturbed distribution function can be solved by orbit integration
(Stix, 1962; Rosenbluth, 1965). In this calculation there is an
applied electric field leading to CE/B drift in the orbits. The
perturbed distributions can then be substituted into Poisson's
equation to get a dispersion relation

$$0 = K^{2} \lambda_{D}^{2} + \frac{1 + \frac{\omega^{*}}{K a_{I}} Z\left(\frac{\omega^{*}}{K a_{I}}\right)}{1 + \frac{i V_{IN}}{K a_{I}} Z\left(\frac{\omega^{*}}{K a_{I}}\right)} + \frac{1 + \sum_{n=-\infty}^{\infty} \Gamma_{n} \frac{\tilde{\omega}}{K_{\parallel} a_{E}} Z\left(\frac{\tilde{\omega} + n \Omega_{E}}{K_{\parallel} a_{E}}\right)}{1 + \frac{i V_{EN}}{K_{\parallel} a_{E}} \sum_{n=-\infty}^{\infty} \Gamma_{n} Z\left(\frac{\tilde{\omega} + n \Omega_{E}}{K_{\parallel} a_{E}}\right)}$$

$$\tilde{\omega} = \omega - \underline{K} \cdot \underline{V_{d}} + i \gamma_{EN} \; ; \qquad \omega^{*} = \omega + i \gamma_{IN}$$

$$\Gamma_{n} = e^{-\mu_{E}} I_{n}(\mu_{E}) \; ; \qquad \mu_{E} = \frac{K_{\perp}^{2} a_{E}^{2}}{2 \Omega_{E}^{2}} \qquad \lambda_{D}^{2} = \frac{k T}{4 \pi N_{0} e^{2}}$$

$$Z(S) = i \int_{0}^{\infty} e^{i S t - \frac{t^{2}}{4}} \, dt$$

$$\Omega_{E} = \frac{e B_{0}}{C m_{-}} \; ; \qquad \Omega_{I} = \frac{e B_{0}}{C m_{+}}$$

- 2 -

Since $V_{IN} \gg \Omega_E$ the orbit integration for the ions reduces those for

straight line orbits and the ion contribution to the dispersion relation

is independent of the magnetic field. If we assume $K_{||}=0$ and $\tilde{\omega} \ll \Omega_E$

the dispersion relation reduces to

$$O = K^2 \lambda_D^2 + \frac{1 + \frac{\omega^*}{Ka_I} Z\left(\frac{\omega^*}{Ka_I}\right)}{1 + \frac{i\gamma_{IN}}{Ka_I} Z\left(\frac{\omega^*}{Ka_I}\right)} + \frac{(1-\Gamma_o)(\omega - K \cdot V_d + i V_{EN})}{\omega - K \cdot V_d + i(1-\Gamma_o)V_{EN}}$$

In the long wavelength approximation $K^2\lambda_D^2$ can be neglected, $1-\Gamma_o$

becomes μ_E, and the dispersion relation reduces to Farley's for $K_{||}=0$.

The roots of the dispersion relation have been solved numerically

by contour integration. This is a standard application of well known

consquences of Cauchy's residue theorem. We will not go into a

discussion of the method here. For an illuminating discussion of

the method, see McCune and Fried (1967).

Figures (1), (2), and (3) illustrate the results of our calcula-

tion. Figure (1) shows the change of growth rate with variation in

electron density. (In the auroral zone the electron density can

vary from quiet to disturbed times by a factor of more than a

hundred.) The growth rate and oscillation frequency were normalized

to the geometric mean gyrofrequency in our calculation but we have

included a scale in kiloHertz for convenience of interpretation. For

small drifts, only long wavelength modes will be unstable. Therefore,

we chose a large value of V_d in the direction of the propagation vector

$\underline{K}$, $\underline{K} \cdot \underline{V}_d / KA_I = 3$, to study the growth rate's dependence on electron

density. In the low frequency region the curves show that electron

Debye length correction is unimportant, in agreement with Farley's

assumption. However, as the electron density of the plasma is increased,

the range of frequency of unstable modes also increases. The most rapidly growing mode shifts to higher frequency with increasing density. There is then a density threshold for destabilizing higher frequency modes; for a value of electron density greater than 1×10^5 cm^{-3}, the range of unstable modes includes the geometric mean gyrofrequency. At this high density the geometric mean gyrofrequency is just the lower hybrid frequency. In general, the upper cutoffs of unstable frequencies lie near but above the density dependent lower hybrid frequency ($\frac{1}{\omega_{LH}^2} = \frac{1}{\omega_{PI}^2} + \frac{1}{\Omega_E \Omega_I}$) at all densities.

Figure (2) illustrates the change in growth rate due to variation of the value of $\underline{V}_d$ projected upon the propagation vector. The results of figure (1) indicates that to generate high frequency waves, a large electron density would be required. For this reason we have chosen $N_E = 3.5 \times 10^5$ cm^{-3}. This is a reasonable value for the auroral electrojet during a magnetic substorm. The result of figure (2) indicates that for a factor 2 increase in drift speed, from $1.5A_I$ to $3.0A_I$ the range of unstable frequency increases rapidly to include frequencies above the geometric mean gyrofrequency, and the most rapidly growing mode shifts to near the geometric mean gyrofrequency.

In figure (3) we have cast our results in a form which may perhaps be useful for backscattering experiments. The dotted curves on the graph represent the normalized phase speed of <u>unstable</u> waves as a function of normalized wavelength for the two indicated values of $\underline{K} \cdot \underline{V}_d / KA_I$. When the wave stabilizes, the dotted curve ends. The phase speed has been defined as W_R / KA_I where W_R is the real part of the complex frequency. The solid curve on the graph is a plot of the critical $\underline{K} \cdot \underline{V}_d / KA_I$ for instability against wavelength. Drifts above

the solid curve are unstable. A scale representing the corresponding
radar frequency for backscattering experiments has been added for
convenience.

From a family of such dotted phase speed curves, a polar plot
of angular distribution of phase speeds relative to the current
direction can be obtained. The solid curve enables us to determine
the angle relative to the current at which the wave stabilizes. In
the upper left hand corner are two examples of such polar plots.
The polar plots correspond to a relative drift of $3A_I$ between the
electrons and ions in the horizontal direction. One feature of the
polar plots is that the angular distribution of phase speed becomes
more isotropic for higher frequency backscattering experiment. On the
other hand, for lower frequency backscattering experiments, the cone
of angles of unstable waves is larger. For the 300 MHz case, the
phase speed varies by a factor of about two as the direction of
propagation vector changes from a direction parallel to the drifting
electrons to the extreme limit of the cone. This would then indicate
that a 300 MHz radar pointing at different directions relative to
the electron drift will observe different Dopplar shifted frequencies.
This prediction disagrees with observations of the equatorial
electrojet (Bowles et al, 1963; Cohen and Bowles, 1967). This
discrepency between prediction and observation may be due to the
effects of nonlinear saturation of the instability. Nevertheless,
a constant Doppler shift in frequency cannot be predicted on the
basis of linear calculation.

The instability mechanism of Buneman (1963) and Farley (1963)
has been well received as a possible explanation for the observations

of long wavelength backscattering in the equatorial electrojet. In addition, a significant number of auroral backscattering experiments have features which of all the proposed mechanisms can best be interpreted in terms of the Buneman-Farley instability (Moorcroft, 1966; and Forsyth, 1968). An interesting feature of the present calculations is that a small increase of a factor 2 in the electron drift shifts the most unstable wave from the long wavelength region, appropriate to most backscattering experiments, to short wavelengths and high frequencies near the geometric mean gyrofrequency. This fact immediately suggests that the high frequency component may have to be taken into account in calculations of the turbulent saturation of the Hall current instability driven beyond threshold.

Our calculations also indicate that, unless nonlinear effects prevent V_d/A_I from approaching 3, VLF electrostatic hiss and short wavelength backscatter ought to accompany strong Hall currents and long wavelength backscatter. On the other hand, when V_d/A_I is small, long wavelength backscatter could be observable without hiss. Thus hiss, backscatter, and electrojet correlation studies might prove interesting.

Finally, we note that Hall currents can generate waves in part of the frequency band appropriate to auroral VLF hiss, which, assuming appropriate conversion to electromagnetic waves, might be related to the apparent correlation of VLF hiss and local auroral electrojet activity (Harang and Larsen, 1965).

Acknowledgments

References

Bowles, K. L., B. B. Balsley, and Robert Cohen, Field-aligned E-region
irregularities identified with accoustic plasma waves, J. Geophys.
Res., 68, 2485-2501, 1963.

Buneman, O., Excitation of field aligned sound waves by electron
streams, Phys. Rev. Letters, 10, 285-287, 1963.

Cohen, R., K. L. Bowles, Secondary irregularities in the equatorial
electrojet, J. Geophys. Res., 72, 885-894, 1967.

Farley, D. T. Jr., A plasma instability resulting in field-aligned
irregularities in the ionosphere, J. Geophys. Res., 68,
6083-6097.

Forsyth, P. A., Radio aurora, a review of research in radio-aurora
for the period 1963-1967, Annales De Geophysique, 555-561, 1968.

Harang, L., R. Larsen, Radio wave emissions in the v.l.f.-band observed
near the auroral zone-I, occurence of emission during dis-
turbances, J. Atmosph. Terr. Phys., 27, 481-497, 1965.

McCune, J. E. and B. D. Fried, The Cauchy-Intergral root-finding
method and the plasma "Loss-Cone" instability, MIT Center
for Space Research, CSR TR-67-1, (January, 1967)

Moorcroft, D. R., The interpretation of the frequency dependence of
radio aurora, Planet. Space Sci., 14, 269-275, 1966.

Rosenbluth, M. N., Microinstablities, In: Plasma Physics, International
Atomic Energy Agency, 1965, p. 485.

Stix, T. H., The theory of Plasma Waves, McGraw-Hill, N. Y., 1962.

Figure Captions

Figure 1. Change in growth rate due to variation in electron density

   For a fixed value of $\underline{K} \cdot \underline{V}_d / KA_I = 3$, ($\underline{K}$ the propagation vector, $\underline{V}_d$ the relative drift velocity between electrons and ions, and A_I the ion thermal speed), the growth rate γ is plotted against oscillation frequency for four different values of electron density. γ and ω_R are normalized to the geomtric mean gyrofrequency. For a magnetic field of .5 gauss an upper scale in kiloHertz is shown for the oscillation frequency. For increasing density, the range of unstable frequencies increases to include frequencies above the geometric mean gyrofrequency.

Figure 2. Change in growth rate due to variation in $\underline{K} \cdot \underline{V}_d / KA_I$

   For a fixed electron density $N_E = 3.5 \times 10^5$ cm^{-3} the growth rate γ is plotted against oscillation frequency ω_R for four different values of $\underline{K} \cdot \underline{V}_d / KA_I$. γ and ω_R are normalized to $\sqrt{\Omega_E \Omega_I}$, the geometric mean gyrofrequency. $\underline{K}$ is the propagation vector, $\underline{V}_d$ is the relative drift velocity between electrons and ions, and A_I is the ion thermal speed. For a magnetic field of .5 gauss, a corresponding scale in kiloHertz is shown for the oscillation frequency. The value of $\omega_{PI}^2 / \Omega_E \Omega_I = 15$ corresponds to the chosen value of N_E and a magnetic field of .5 gauss. For an increase of a factor 2 in electron drift the range of unstable frequencies increases to include frequencies above the geometric mean gyrofrequency and the fastest growing mode shifts to high frequency, near the geometric mean gyrofrequency.

Figure 3. Phase speed and critical value of electron drift as a

function of wavelength

For fixed temperature $T = 230°K$ and electron density $N_E = 3.5 \times 10^5 cm^{-3}$
the dotted curves on the graph are plots of normalized phase speed
W_R/KA_I of <u>unstable</u> waves versus normalized wavelength for two
different values of $\underline{K} \cdot \underline{V}_d/KA_I$. The dotted curve ends when the wave
becomes stable. W_R = real part of the complex frequency, $\underline{K}$ = propagation
vector, $\underline{V}_d$ = relative drift velocity between electrons and ions,
A_I = ion thermal speed, A_E = electron thermal speed, and Ω_E = electron
cyclotron frequency. A scale representing the corresponding radar
frequency for backscattering experiment is also shown. Also on the
same graph and using the same vertical scale is a plot of critical
$\underline{K} \cdot \underline{V}_d/KA_I$ versus normalized wavelength. For various values of $\underline{K}$,
the drift velocities giving $\underline{K} \cdot \underline{V}_d/KA_I$ values greater than those
of the solid curve, the corresponding waves become unstable. In
the upper corner are polar plots of angular distribution of phase
speed relative to the direction of electron drift for the two indicated
radar frequencies. The length of the arrows represent the magnitudes
of W_R/KA_I. The relative drift V_d between electrons and ions in
the horizontal direction has a magnitude of $3A_I$.
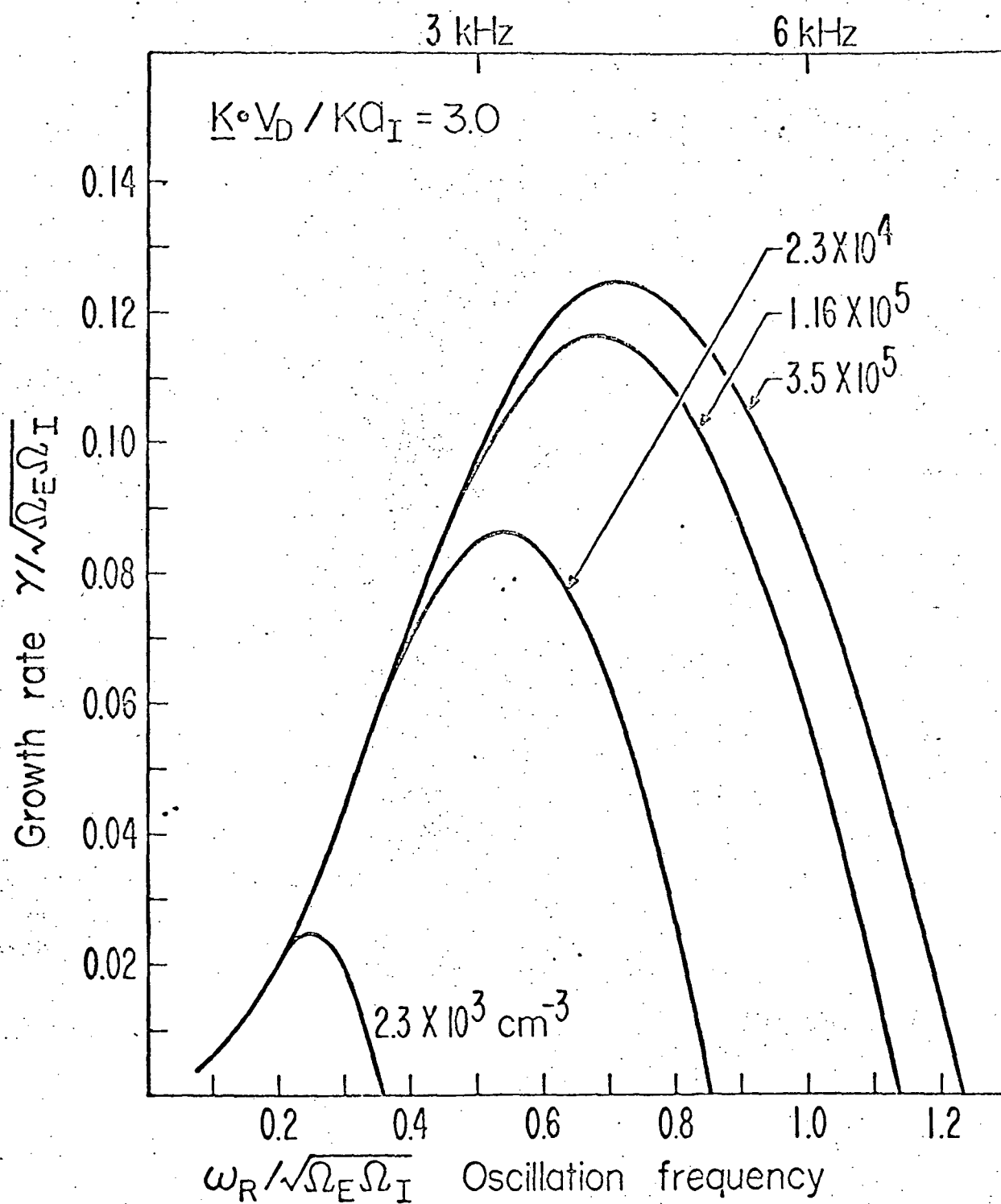
Change in growth rate due to variation in electron density

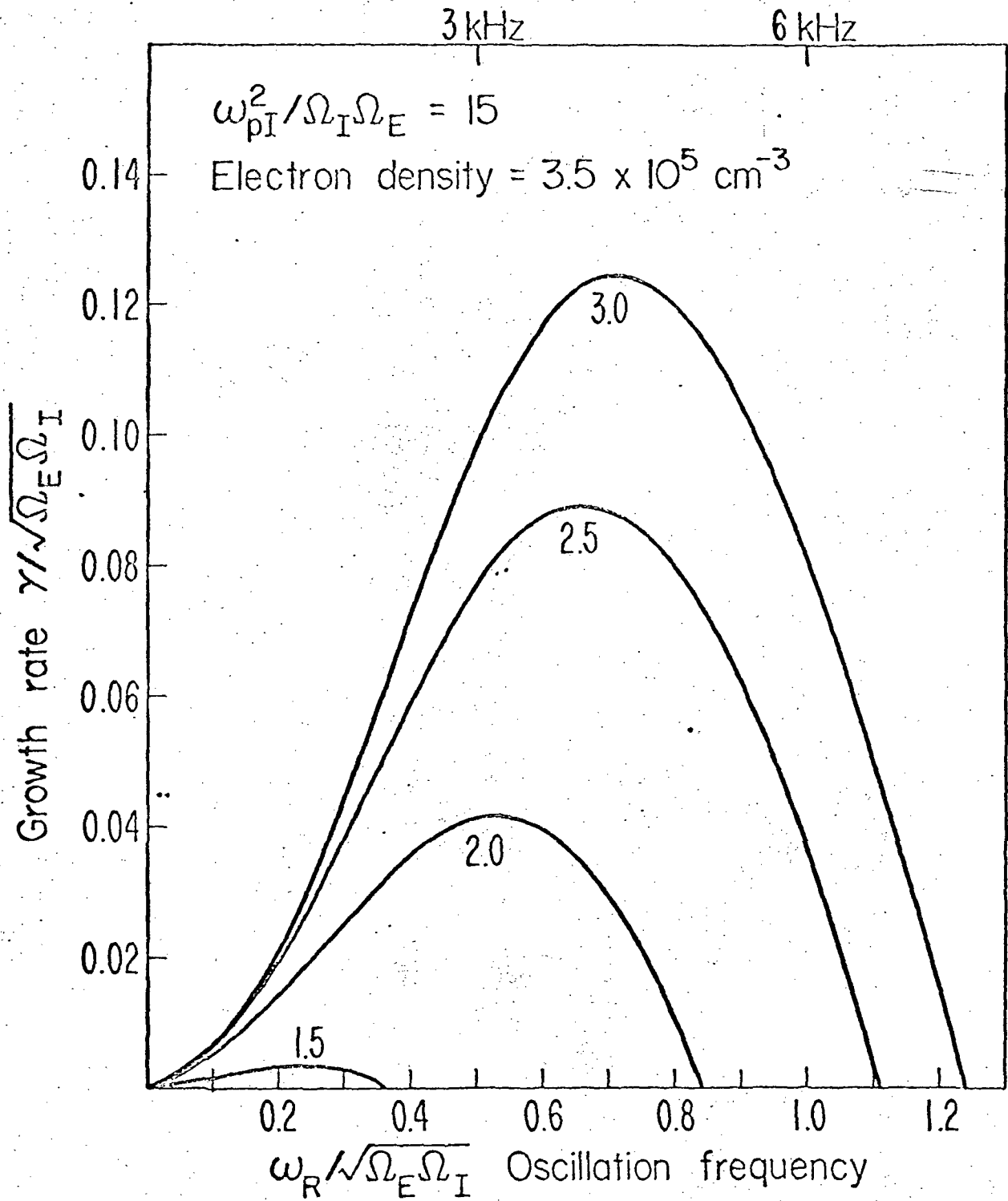FIGURE (1)

Change in growth rate due to variation in

$$\underline{K} \circ \underline{V}_D / K a_I$$

FIGURE (2)

FIGURE (3)

$N_E = 3.5 \times 10^5 \ cm^{-3}$

$T = 230 \ ^\circ K$

$V_D = 3a_I$

$\dfrac{K \cdot \underline{V}_D}{Ka_I} = 3$

$\dfrac{K \cdot \underline{V}_D}{Ka_I} = 2$

critical $\dfrac{K \cdot \underline{V}_D}{Ka_I}$

$K^2 \rho_E^2 = K^2 a_E^2 / 2\Omega_E^2 \ ;$

phase speed ω_R / Ka_I

UNSTABLE

STABLE

300 MHz

1000 MHz

400   1000   800   1000   1500   MHz